Biochimica et Biophysica Acta 1838 (2014) 319–327

Contents lists available at ScienceDirect

Biochimica et Biophysica Acta

journal homepage: www.elsevier.com/locate/bbamem

Importance of polarity of the α4–α5 loop residue—Asn^{166} in the pore-forming domain of the *Bacillus thuringiensis* Cry4Ba toxin: Implications for ion permeation and pore opening

Thanate Juntadech [a,1], Yodsoi Kanintronkul [a,1], Chalermpol Kanchanawarin [c], Gerd Katzenmeier [a], Chanan Angsuthanasombat [a,b,*]

[a] Bacterial Protein Toxin Research Cluster, Institute of Molecular Biosciences, Mahidol University, Salaya Campus, Nakornpathom 73170, Thailand
[b] Laboratory of Molecular Biophysics and Structural Biochemistry, Biophysics Institute for Research and Development (BIRD), Nakornpathom 73170, Thailand
[c] Laboratory of Theoretical and Computational Biophysics, Department of Physics, Faculty of Science, Kasetsart University, Bangkok 10900, Thailand

ARTICLE INFO

Article history:
Received 2 August 2013
Received in revised form 1 October 2013
Accepted 3 October 2013
Available online 10 October 2013

Keywords:
Bacillus thuringiensis
Cry δ-endotoxins
Dye-leakage assay
MD simulations
Planar lipid bilayers
Trimeric pore

ABSTRACT

Bacillus thuringiensis Cry4Ba toxin is lethal to mosquito-larvae by forming ion-permeable pores in the target midgut cell membrane. Previously, the polarity of Asn^{166} located within the α4–α5 loop composing the Cry4Ba pore-forming domain was shown to be crucial for larvicidal activity. Here, structurally stable-mutant toxins of both larvicidal-active (N166D) and inactive (N166A and N166I) mutants were FPLC-purified and characterized for their relative activities in liposomal-membrane permeation and single-channel formation. Similar to the 65-kDa trypsin-activated wild-type toxin, the N166D bio-active mutant toxin was still capable of releasing entrapped calcein from lipid vesicles. Conversely, the two other bio-inactive mutants showed a dramatic decrease in causing membrane permeation. When the N166D mutant was incorporated into planar lipid bilayers (under symmetrical conditions at 150 mM KCl, pH 8.5), it produced single-channel currents with a maximum conductance of about 425 pS comparable to the wild-type toxin. However, maximum conductances for single K^+-channels formed by both bio-inactive mutants (N166I and N166A) were reduced to approximately 165–205 pS. Structural dynamics of 60-ns simulations of a trimeric α4–α5 pore model in a fully hydrated-DMPC system revealed that an open-pore structure could be observed only for the simulated pores of the wild type and N166D. Additionally, the number of lipid molecules interacting with both wild-type and N166D pores is relatively higher than those of N166A and N166I pores. Altogether, our results further signify that the polarity at the α4–α5 loop residue—Asn^{166} is directly involved in ion permeation through the Cry4Ba toxin-induced ionic pore and pore opening at the membrane–water interface.

1. Introduction

Cry insecticidal proteins known as δ-endotoxins are produced in the form of crystalline inclusions during sporulation by the Gram-positive soil bacterium *Bacillus thuringiensis* (*Bt*). These crystal toxins are cytolytic pore-forming toxins that are lethal to various insect larvae [1]. For example, Cry4Aa and Cry4Ba, two closely related δ-endotoxins made by *Bt* subsp. *Israelensis* (*Bti*), are highly toxic to the larvae of *Aedes* and *Anopheles* mosquitoes, vectors of dengue viruses and malaria, respectively [2–4]. Biochemically, the Cry inclusions are solubilized in the midgut lumen of susceptible insect larvae at alkaline pH for both dipterans and lepidopterans, and proteolytically activated by gut proteases to yield the active toxins of ~65-kDa. Subsequently, the activated toxins bind specifically to a variety of receptors such as GPI (glycosylphosphatidyl inositol)-anchored aminopeptidase-N and GPI-anchored alkaline phosphatase that are found on the brush-border membrane (BBM) of midgut epithelial cells [5,6]. This toxin-receptor interaction could assist toxin penetration into the cell membrane, leading to the formation of ion-permeable pores that eventually cause osmotic lysis of the target cells. Although our understanding of toxic mechanisms of *Bt*-Cry toxins has expanded dramatically over the last decade [1,3,6], their exact mechanisms of action at the molecular level still remain to be explored.

We now know the crystal structures of a number of *Bt*-Cry toxins [7–11], including the *Bti*-Cry4Ba mosquito-active toxin (Fig. 1A). Despite their broad diversity in insecticidal spectra, all the known Cry structures of the 65-kDa activated form reveal a high degree of overall structural conservation, suggesting that they all employ a common mode of action. The structures display a distinct three-domain arrangement (an α-helical bundle, a three-β-sheet assembly and a β-sandwich) which resembles a wedge-shaped body with size of about 55 × 65 × 75 Å [3,9]. Of particular interest, it is structurally obvious that the helical domain

* Corresponding author at: Bacterial Protein Toxin Research Cluster, Institute of Molecular Biosciences, Mahidol University, Salaya Campus, Nakornpathom 73170, Thailand.
E-mail address: chanan.ang@mahidol.ac.th (C. Angsuthanasombat).
[1] Authors with equal contributions.

0005-2736/$ – see front matter © 2013 Elsevier B.V. All rights reserved.
http://dx.doi.org/10.1016/j.bbamem.2013.10.002

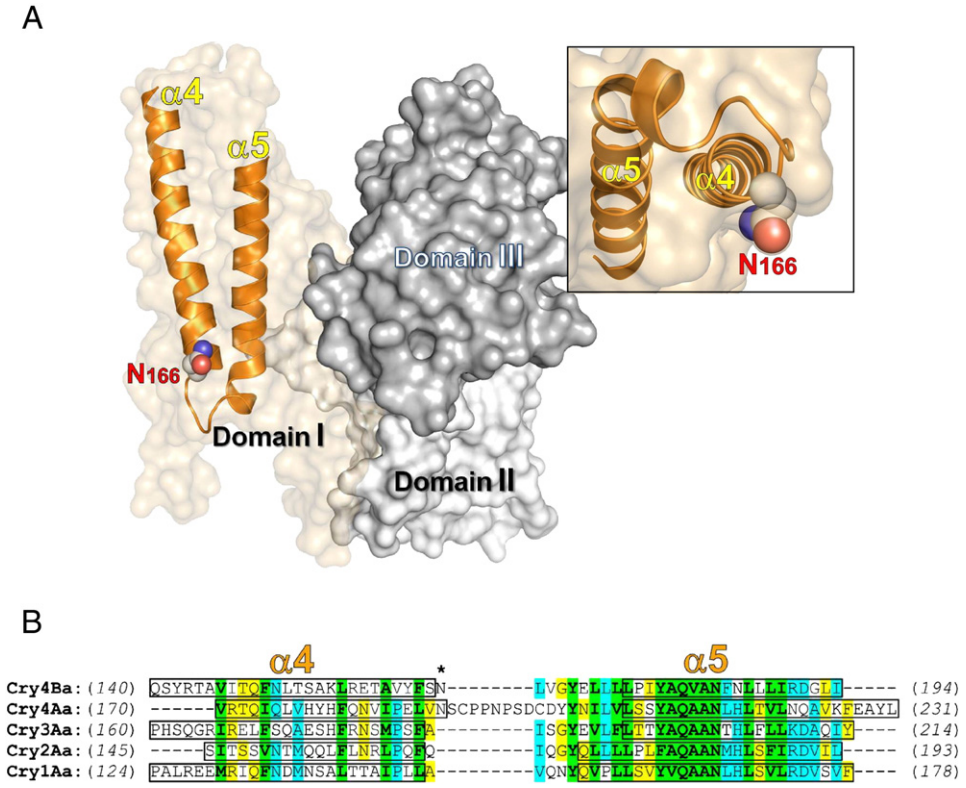

Fig. 1. The Cry4Ba crystal structure and its Asn[166] location. (**A**) Surface representation of the three-domain Cry4Ba toxin organization (domains I–III), illustrating the α4-loop-α5 hairpin (schematic ribbon) within the pore-forming domain (domain I) with the location of Asn[166] drawn as vdW (van der Waals) spheres. Inset, a zoom-in bottom view of the exposed Asn[166] residue. The structure was generated by using PyMOL program. (**B**) Sequence alignments of the α4-loop-α5 hairpin of Cry4Ba [7] with those of four other known Cry structures, Cry4Aa [8], Cry3Aa [9], Cry2Aa [10] and Cry1Aa [11]. Corresponding α4 and α5 of all known structures are illustrated as rectangular blocks connected by loop sequences. Note that the position of Cry4Ba-Asn[166] (denoted by *) corresponds most closely to that of Cry4Aa-Asn[190] which was previously substituted with Ala, but showing no effect on the toxin activity [23].

is likely to be a transmembrane pore-forming unit, given that at least five helices, *i.e.* α3, α4, α5, α6 and α7, are of sufficient length (>30 Å) to span the lipid membrane [3,9]. Additionally, this helical domain has been experimentally proven capable of membrane-inserted pore formation, albeit in the absence of specific receptors [11–14].

Nonetheless, the precise structural feature of such a Cry toxin-induced pore is not yet known. At present, it seems that the so-called "umbrella-like" model is still the most well-known description for depicting the membrane-insertion and pore-formation stages of the three-domain Cry toxins [15,16]. This proposed model entails an insertion of the two pore-lining helices, *i.e.* α4 and α5, into the lipid membrane as a helical hairpin arrangement, and in so doing the remaining helices spread over the membrane surface like the opening of an umbrella [16]. Substantial evidence has preferentially supported this mechanistic model by signifying the role of both α4 and α5 in the toxicity of different Cry toxins [17–20]. For instance, numerous studies of Cry toxin-induced pore formation suggested that α4 lines the pore lumen and plays a part in ion conduction [17,18], while α5 is rather hydrophobic and could take part in toxin-pore oligomerization [19,20].

In our earlier study, we provided direct evidence for liposomal membrane-permeating activity of the α4-loop-α5 fragment purified from the engineered Cry4Ba toxin [21]. Similar studies by other workers *via* the use of synthetic peptides corresponding to α4, α5 and α4-loop-α5 of Cry1Ac clearly demonstrated that the loop linking α4 and α5 is basically required for efficient penetration of these two transmembrane helices into the lipid bilayers to induce membrane permeabilization [22]. This notion was supported by our results that revealed a structural requirement for larvicidal activity of one highly conserved aromatic residue found within the α4–α5 loop of both Cry4Aa (Tyr[202]) and Cry4Ba (Tyr[170]), conceivably for stabilizing the membrane-associated pore complex [23,24]. Other workers showed that one Cry1Aa mutant, Y153D, in which the conserved aromatic residue—Tyr[153] in the α4–α5 loop region (corresponding to Cry4Aa-Tyr[202] or Cry4Ba-Tyr[170]), exhibited a loss in larvicidal activity due to its inability to incorporate into BBM vesicles [25]. Likewise, two other conserved aromatic residues (*i.e.* Tyr[249] and Phe[264]), which are oriented on the same side of Cry4Ba-α7, were also found to be important for larvicidal activity [26]. The conserved helix 7 may undergo a conformational change to convert into a membrane-inserted β-hairpin which acts as a lipid anchor needed for membrane penetration by the pore-forming α4-loop-α5 [27].

We have also demonstrated that the polarity of Cry4Ba-Asn[166] placed within the α4–α5 loop region (Fig. 1) is necessary for larvicidal activity [24]. Herein, fluorescence dye-leakage assays as well as single-channel analysis were employed to further characterize both larvicidal-active and inactive Cry4Ba-Asn[166] mutants for their potential activities in liposomal-membrane permeabilization and ion-channel formation. MD simulation trajectories for a trimeric α4-loop-α5 pore of Cry4Ba and its mutants in a fully hydrated DMPC (1,2-dimyristoyl-*sn*-glycero-3-phosphocholine) bilayer system were also generated to study their structural stability and dynamics. As a whole, our present data clearly signified for the first time that the polarity (not the side chain *per se*) of the α4–α5 loop residue—Asn[166] in the Cry4Ba pore-forming domain has important implications for both ion permeation and pore opening at the membrane–water interface.

2. Materials and methods

2.1. Toxin expression, solubilization, activation and purification

Cry4Ba wild-type and its Asn[166] mutant toxins were over-expressed in *Escherichia coli* JM109 upon induction with isopropyl-β-D-thiogalactopyranoside (0.1 mM final concentration) as described

previously [24]. Toxin inclusions (1–2 mg/mL), which were centrifugally purified from French Press-disrupted lysates, were solubilized by incubation at 37 °C for 1 h in carbonate buffer (50 mM Na_2CO_3/$NaHCO_3$, pH 9.0). Solubilized protoxins were then activated with trypsin (tolylsulfonyl phenylalanyl chloromethyl ketone-treated; Sigma) at a ratio of 1:20 enzyme/toxin (w/w) at 37 °C for 16 h. After SDS-PAGE (sodium dodecyl sulfate-polyacrylamide gel electrophoresis) analysis, the trypsin-treated fraction was concentrated by ultrafiltration (30-kDa cutoff) and further purified by a size-exclusion FPLC system (Superose™ 12 column; GE Healthcare Life Biosciences) eluted with the carbonate buffer (pH 9.0) as described elsewhere [28]. Protein concentrations were determined using the Bradford-based protein microassay (Bio-Rad), with bovine serum albumin (BSA fraction V; Sigma) as a standard protein.

2.2. Larvicidal activity assays

Bioassays for mosquito-larvicidal activity were done at room temperature (~25 °C) for 24 h using 2 day-old *Aedes aegypti* larvae as described previously [18]. The assays were carried out in a 48-well polystyrene plate (11.3-mm well diameter) with 1 mL/well of toxin inclusion suspension (5 μg/mL suspended in distilled water). 100 larvae (10 larvae/well × 10 wells) were used for treatment with each toxin sample. Statistical analyses were carried out by using one-way analysis of variance (ANOVA) tests *via* SigmaStat v2.0 for comparing all the group means. The Tukey multiple comparison test among pairs of group means [29] was performed as post tests to determine which groups are significantly different from other groups. Probabilities (p values) <0.05 were considered as being significant.

2.3. Circular dichroism (CD) measurements

CD spectra of the purified trypsin-treated toxins were measured with a Jasco J-715 spectropolarimeter (calibrated with a solution of camphorsulfonic acid), scanned in the far UV region (185–280 nm) at 25 °C using a rectangular quartz cuvette (0.2-mm path length) as described previously [26]. Protein samples were prepared in sodium phosphate buffer (50 mM NaH_2PO_4/Na_2HPO_4, pH 9.0), with concentrations of 0.30–0.50 mg/mL, as determined by far UV absorbance. CD measurements were recorded at a rate of 50 nm/min with a spectral bandwidth of 2 nm. CD signals (mdeg), which were averaged from at least five accumulations and then corrected for solvent baseline, were finally converted to mean residue ellipticity ([θ], deg·cm^2/dmole).

2.4. Lipid vesicle preparation and fluorescence dye-leakage assays

Large unilamellar vesicles (LUVs, mean diameter of about 100 nm) encapsulated with calcein (C-481; Molecular Probes) at a self-quenching concentration of 60 mM in 50 mM Na_2CO_3/$NaHCO_3$, pH 9.0, were prepared from a lipid mixture (Avanti Polar Lipid) of phosphatidylcholine (PC), phosphatidylethanolamine (PE), and cholesterol (Ch) (10:10:1, w/w) by the extrusion method according to standard procedures described previously [21]. Suspension concentrations of calcein-loaded LUVs (in 150 mM NaCl, 50 mM Na_2CO_3/$NaHCO_3$, pH 9.0) were estimated by measuring the lipid phosphorus content [30], and a final concentration of 2.5 μM was used for calcein leakage assays [21].

Release of entrapped calcein was monitored as function of time t by measuring an increase in fluorescence emission at 520 nm (excitation 495 nm) on a LS50 spectrofluorometer (Perkin-Elmer) at 25 °C. Efflux curves were normalized to percentage of release activity or fluorescence recovery F_t which is defined as $F_t = (I_t - I_0) / (I_{max} - I_0) \times 100$, where I_0 is the initial fluorescence intensity, I_{max} is the total fluorescence intensity observed upon addition of Triton X-100 (causing 100% calcein leakage) and I_t is the fluorescence intensity observed after adding the tested toxins at time t. For the concentration–activity profile, the plot of fractional release activity $Y(P_{TL} / 1 - P_{TL})$ *versus* toxin concentration [T] was fitted to the Hill equation, $P_{TL} / 1 - P_{TL} = [T]^n / EC_{50}$, where P_{TL} is the probability of finding toxin–liposome complex T_nL to give the Hill coefficient n and the effective concentration EC_{50}.

2.5. Planar lipid bilayers (PLBs) and single channel analysis

PLBs were formed at 25 °C by painting a 7:2:1 (w/w) lipid mixture of PE, PC, and Ch on a 200-μm aperture in a 1 mL-Delrin cup, with membrane capacitance values of 200–250 pF as described earlier [31]. Toxin incorporation (at amounts of ~20 μg/mL) was facilitated by stirring the protein-containing buffer (150 mM KCl, 10 mM Tris–HCl, pH 8.5) in the *cis* chamber while applying a 100-mV holding potential across the lipid bilayer. Single-channel currents were recorded with an Axopatch-1D amplifier (Axon Instruments). Signals, which were low-pass filtered at 600 Hz, were digitized with a Digidata 1200 analog-to-digital converter using Axoscope 8.0 software (Axon Instruments) at a 50-kHz sampling frequency. Channel conductances were determined from the slope of current–voltage (I–V) relations plotted between the observed current steps and the corresponding applied voltage.

2.6. Pore modeling and molecular dynamics (MD) simulations

A 3D model of a trimeric pore consisting of α4-loop-α5 hairpins of Cry4Ba extracted from the X-ray trimer structure (PDB ID 1W99) [7] was initially constructed *via* protein docking between the two helices, α4 and α5, using the Hex program [32]. The pore model was inserted into a DMPC (1,2 dimyristoyl-*sn*-glycero-3-phosphocholine) bilayer constructed by using the membrane builder module from the CHARMM GUI server [33]. Two water layers and sodium and chloride ions were added to the DMPC bilayer model using the VMD program [34]. The final pore model in the water/lipid system consisted of three α4–α5 hairpins (34,575 atoms) in a bilayer of 114 DMPC lipids, 5991 water molecules, 15 Na^+ ions and 18 Cl^- ions. The system was energy minimized for 10,000 steps, then heated from temperature 0 to 300 K for 100 ps, equilibrated at pressure of 1 atm for 5 ns and then ran as the final production for 60 ns using the NAMD program [35] running on a computer with 8 CPUs at 1 ns/day.

The equilibrated coordinates of the 5-ns wild-type pore system were used as a template for MD simulations of the mutant systems. Asp, Ala and Ile were substituted respectively for Asn^{166} in the pore model using the VMD program. Three more sodium ions were added to N166D pore model to neutralize the system. The three pore models of Cry4Ba mutants were energy minimized for 1000 steps, then heated to 300 K for 20 ps, equilibrated at 1 atm for 10 ps, and finally ran as unrestrained molecular dynamics simulations for 60 ns. Analyses of MD trajectories were done *via* the VMD program.

3. Results and discussion

3.1. Larvicidal and biochemical characteristics of Cry4Ba-Asn^{166} mutant toxins

One biologically critical residue, *i.e.* Asn^{166} which is located within the loop connecting the transmembrane helices (α4 and α5) composing the pore-forming domain of the Cry4Ba toxin (Fig. 1) was previously identified by PCR-based directed mutagenesis [24]. Specific substitutions of Asn^{166} with polar uncharged or charged residues, *i.e.* Gln, Cys, Asp or Arg, could retain high toxicity against *A. aegypti* mosquito-larvae comparable to the wild type, whereas replacements with non-polar amino acids, *i.e.* Ala or Ile, almost totally abolished the larvicidal activity, suggestive of functional importance of the polarity of this α4–α5 loop residue [24]. In the present study, toxin inclusions which were purified from particularly selected mutants, *i.e.* N166A, N166I and N166D (Fig. 2A, inset), were used instead to assess their relative

toxicity. The data confirmed that the polarity of Cry4Ba-Asn^{166} placed within the α4–α5 loop is necessary for larvicidal activity (Fig. 2A).

As previously verified, the 130-kDa Cry4Ba protoxins of the wild type and the three mutants (N166A, N166I and N166D) were all cleaved by trypsin into two protease-resistant polypeptides of ~47 and ~20 kDa, in addition to the removal of the ~65-kDa C-terminal half [24]. Herein, upon purification by size-exclusion FPLC chromatography, the trypsin-treated fragments (*i.e.* ~47 and ~20 kDa) of the three mutant toxins (Fig 2B, inset) were found non-covalently associated with each other, forming a 65-kDa protein complex similar to the wild type under non-denaturing conditions used (50 mM Na_2CO_3/$NaHCO_3$, pH 9.0) and eluted from the column in a single peak corresponding to the retention time of the 66-kDa BSA protein marker.

To further determine if each substitution would induce structural changes in the Asn^{166} mutant proteins, the sum of the secondary structure components of the three FPLC-purified mutant toxins, N166A, N166I and N166D, was studied by far-UV CD spectroscopy in comparison with that of the purified wild-type toxin. As shown in Fig. 2B, all the CD spectral profiles between 200 and 270 nm are typically similar, indicating that no drastic changes in the secondary structure elements had occurred in consequence of these three mutations. However, a more positive peak at around 198 nm was observed for the N166D mutant in particular. Although this might imply some local adjustment in the mutated region, the mutation did not seem to give rise to serious structural consequences. This result is consistent with the data from toxin solubilization and trypsin-digesting susceptibility assays as demonstrated earlier, confirming that such mutations did not cause conformational changes of the N166A, N166I and N166D mutant proteins. These results verified that the loss in larvicidal activity observed for both N166A and N166I mutants (Fig. 2A) is least likely to be due to protein misfolding after substitutions with either of these two hydrophobic side-chains.

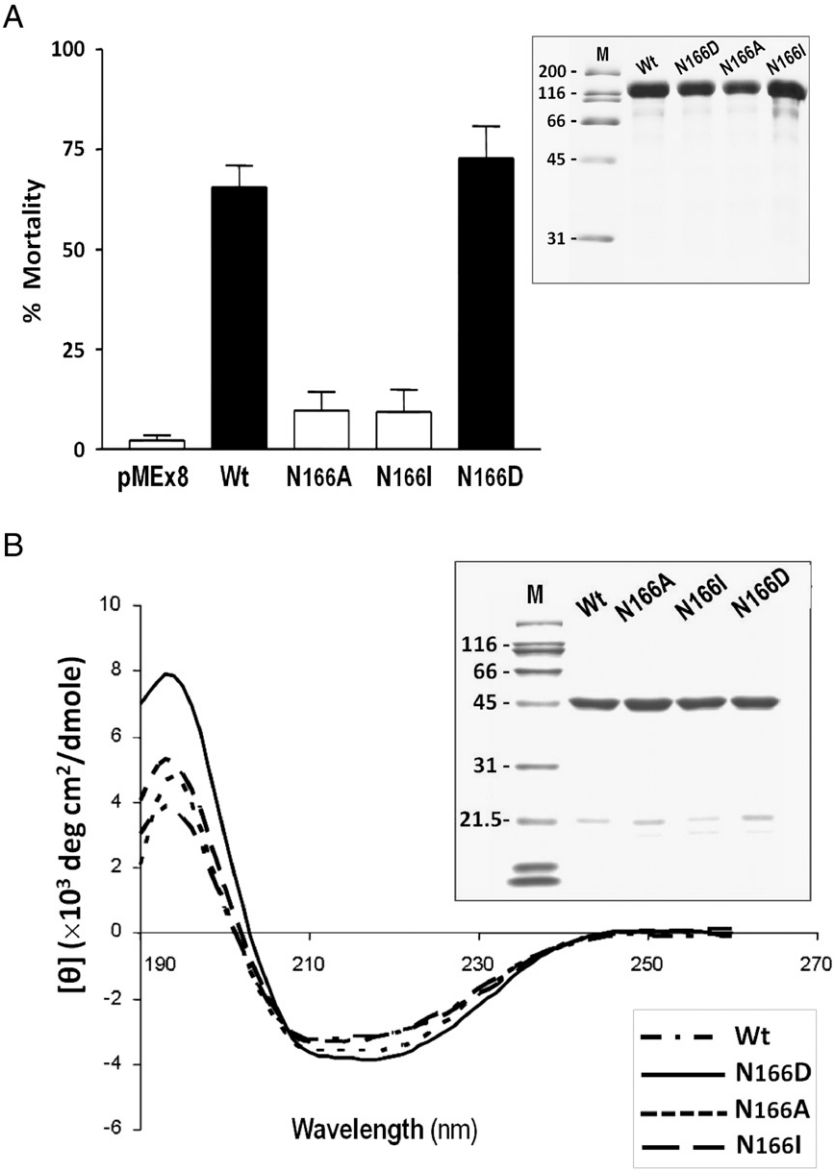

Fig. 2. Larvicidal and biochemical features of Cry4Ba-Asn^{166}-mutants. (**A**) Comparison of larvicidal activities between the Cry4Ba wild-type (Wt) and its Asn^{166} mutant toxins (N166A, N166I, and N166D) against *A. aegypti* mosquito-larvae using purified inclusions (5 μg/mL). pMEx8 represents a negative control: *E. coli* lysate containing the plasmid vector. Error bars indicate standard errors of the mean (SEM) from at least three independent experiments. Unshaded boxes represent the larvicidal activity of the mutants (N166A and N166I) that are very significantly different (p values < 0.001) from that of the wild type and the bioactive mutant (N166D), but not statistically different (p values > 0.05) from the negative control (pMEx8). Inset, SDS-PAGE analysis of purified inclusions, showing 130-kDa wild-type and its mutant protoxins (5 μg/lane). M, molecular mass standards. (**B**) CD spectra of the 65-kDa purified Cry4Ba toxin in comparison with that of the three mutants, N166A, N166I and N166D. Inset, SDS-PAGE analysis of the 65-kDa Cry4Ba wild-type and its mutant toxins after trypsin activation and FPLC-purification, showing two non-covalently associated fragments of ~47 and ~20 kDa.

3.2. Membrane permeability of dye-loaded LUVs induced by Cry4Ba and its mutant toxins

To examine the effect of the Cry4Ba-Asn^{166} mutant toxins on membrane permeability, encapsulated calcein-leakage assays were employed to assess the toxin-induced permeabilization of LUVs whose composition used (PC/PE/Ch, 10:10:1, w/w) is similar to insect cell membranes [36]. Release of the entrapped calcein by individual tested toxins was semi-empirically quantified as the relative increase in fluorescence de-quenching intensity (Fig. 3).

Release activity of the 65-kDa purified wild-type toxin against the calcein-loaded LUVs was at first evaluated at different protein concentrations, and the concentration-*versus*-release activity profile was generated (Fig. 3A). The leakage of trapped calcein increased sigmoidally with toxin concentration, *i.e.* only a small release was observed at low concentrations, but then rather steeply at higher concentrations. This indicates that LUVs were not permeabilized until a critical toxin monomer/vesicle ratio was accomplished. Kinetics of toxin-pore formation are reflected in the dependence of fractional activity (Y) on the Cry4Ba toxin concentration as described in the logarithmic form of the Hill equation, $\log Y = n \log [T] - \log EC_{50}$. The Hill coefficient ($n$) for the tested toxin was determined by fitting the nonlinear concentration–activity profile into the Hill equation (Fig. 3A, inset). For the 65-kDa Cry4Ba activated toxin in LUVs, at pH 9.0, the value of n was found to be about 1.3. Thus, it would conceivably require more than one molecule of the activated toxin to form a functional pore structure in this insect mimetic liposome. It was observed previously that a mixture of Cry4Ba toxin monomers, dimers and trimers is present in liposomes, whereby trimeric species predominantly appear after prolonged incubation of toxin-lipid vesicle [20]. The present results are also in agreement with our previously reported electron crystallographic data at a 17 Å resolution, which demonstrated a horizontal arrangement of three Cry4Ba molecules per membrane-associated pore complex in 2D (two-dimensional) crystals [37].

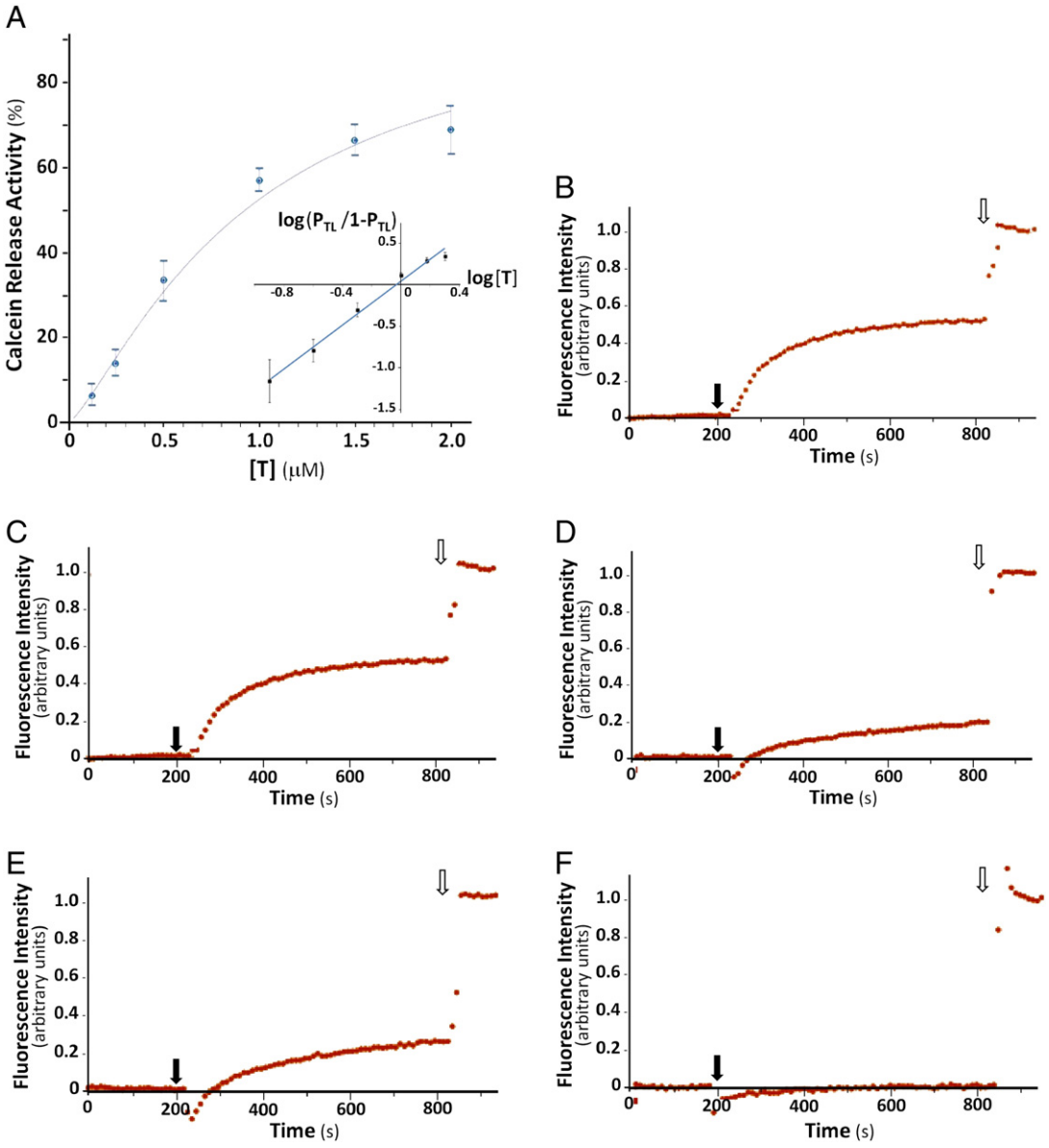

Fig. 3. Effect on membrane permeability of calcein-loaded liposomes by Cry4Ba and its Asn^{166}-mutants. (**A**) Dose response curve for membrane permeability induced by the 65-kDa Cry4Ba wild-type toxin. Inset, the plot of fractional release activity $Y(P_{TL} / 1 - P_{TL})$ *versus* toxin concentration [T]. Error bars indicate SEM from two independent experiments in which each toxin concentration was done in triplicate. (**B**–**F**) Traces represent fluorescence intensity as function of time t after adding Cry4Ba or its Asn^{166} mutants (60 μg/mL). The maximum release was obtained by adding 0.1% triton X-100 (white arrows) after a 10 min-incubation with individual tested toxins (black arrows); (**B**) Cry4Ba wild type, (**C**) N166D, (**D**) N166I, (**E**) N166A, and (**F**) the carbonate buffer (negative control).

In addition, the effective toxin concentration required for 50% dye release (EC_{50}) was also obtained from the curve fitted to the Hill equation. The calculated EC_{50} value for the Cry4Ba wild-type toxin against the calcein-loaded vesicles was found to be ~0.95 μM, which is comparable to that of the larvicidal-active N166D mutant, as both were observed within 10 min (Fig. 3B, C). However, both larvicidal-inactive mutants, N166A and N166I (at concentrations of 0.95 μM or ~60 μg/mL) were much less active in inducing the leakage of the calcein-loaded vesicles, with a maximally observed release of only 20% (Fig. 3D, E), whereas the control showed no effect on dye-leakage (Fig. 3F), indicating that the leakage of calcein did not occur as a result of instability of the vesicle membrane. Taken together, the results substantiate that the polarity of this α4–α5 loop residue—Asn^{166} is required for membrane-pore formation, and therefore a prerequisite for larvicidal activity (see Fig. 2A).

3.3. Ion-channel characteristics formed by Cry4Ba and its Asn^{166}-mutant toxins

Further attempts were made to determine if each single-mutation at Asn^{166} causes an adverse effect on the toxin's ability to form ion channels on PLBs. After about 30-40 min following the addition of individual toxins under symmetrical ionic conditions (at 150 mM KCl, 10 mM Tris–HCl, pH 8.5), the Cry4Ba wild-type and all three mutants (at doses of 0.3 μM or ~20 μg/mL) were able to induce single channel currents at voltages between −100 and +100 mV, as shown by representative current traces in Fig. 4A. However, the capability to produce ion channels was found to be reduced in the two non-toxic mutant proteins, *i.e.* N166A, and N166I, but not in the larvicidal-active N166D mutant, as compared with the wild-type toxin. In agreement with previous reports of ours on Cry4Ba and other workers on Cry toxins [11,12,14,31,38], several distinct sub-conductance levels were frequently detected for all tested toxins. These observations are suggestive of a multimeric manner of toxin incorporation into the lipid bilayer. Like other ion channels [39,40], the Cry toxin-induced channels would perhaps go through conformational rearrangements during channel gating. Although at present a possible gating mechanism for the channels induced by Cry toxins has not yet been unambiguously demonstrated, PLB experiments suggest that, in analogy to known channel-forming toxins [41], Cry toxin-induced channels could exhibit closed and open functional states [11,12,14,31,38].

As shown in Fig. 4B, the current–voltage relations of all single channels formed by the wild-type and mutant toxins are linear revealing maximum conductances ranging from ~150 to ~450 pS. Consistent with the dye-leakage results, the maximum conductance of the bioactive N166D mutant (425.5 ± 6.5 pS, n = 4) was found to be comparable to that of the wild-type toxin (450.5 ± 25.5 pS, n = 4). However, both the non-toxic mutants, N166A and N166I, exhibited about a half lower conductance (165.0 ± 5.5 pS, n = 5 and 205.5 ± 14.5 pS, n = 4, respectively). These results suggest that the α4–α5 loop residue (Asn^{166}) is involved in regulating the passage of ions through the channel pore. The data also imply that the polarity but not the type of amino acid side-chain at position-166 is an important determinant for ion permeation and conduction in the Cry4Ba-induced channels.

3.4. Structure and dynamics of Cry4Ba α4–α5-induced pore models in bilayers

Currently, the number of toxin monomers that constitute a functional pore complex within the lipid membrane is still under debate. Previous studies have reported the existence of trimeric as well as tetrameric complexes of toxin monomers [37,42–44]. A trimeric organization of the 65-kDa activated Cry4Ba toxin in association with lipid membranes as revealed by 2D crystallographic analysis was described recently [37]. Here we performed MD simulations of a trimeric α4–α5 pore of Cry4Ba

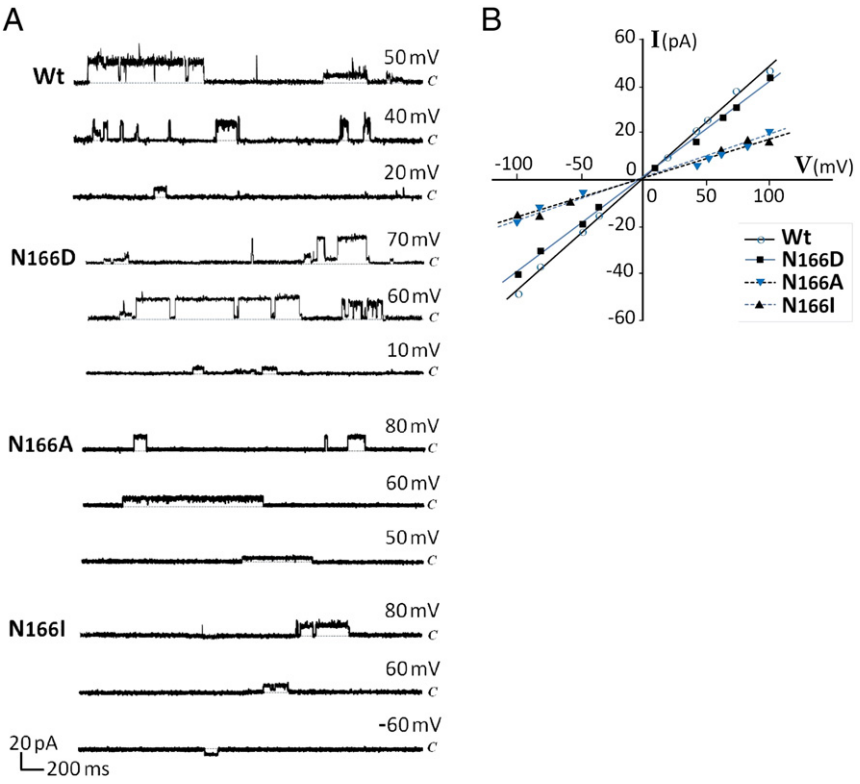

Fig. 4. Ion-channel properties of Cry4Ba and its Asn^{166}-mutant toxins. (**A**) Current traces recorded after partition of the 65-kDa purified Cry4Ba wild-type (Wt) and its mutant toxins—N166D, N166A and N166I (20 μg/mL) into PLBs under symmetrical conditions (150:150 mM KCl *cis*:*trans*). Applied voltages are indicated on the right side of each trace. The close stage level of the channel is denoted by the letter *c*. Vertical and horizontal bars indicate measured current-time scales, respectively. (**B**) Current-voltage relations obtained from the single-currents recorded under symmetric conditions.

and its three Asn^{166} mutants (N166A, N166I and N166D) in a DMPC bilayer for 60 ns to study their conformational dynamics. During the simulation-time interval of 60 ns, the wild-type pore visibly opened up as shown in Fig. 5A–D. By simple geometry, the pore diameter (D) at time $t = 60$ ns could be estimated from the average separation distance d ~25 Å, as $D = d / \sqrt{3} \approx 25 / \sqrt{3} \approx 14.4$ Å. The calculated pore size is large enough for calcein with a hydrodynamic-Stokes diameter of ~13 Å [45] to pass through as demonstrated above in the dye-leakage experiments (see Fig. 3). The data are also in agreement with a pore diameter of ~20 Å as estimated from polyethylene glycol-blockage PLB experiments for Cry1Ca [14].

Initial size and dynamics of the trimeric pores formed by the wild type and its mutants were obtained from their alterations in the average separation distance d (C_α to C_α) between three Asn^{166} residues on each individual pore (Fig. 5E). It can be seen that the trimeric pores of N166A and N166I mutants did not open up, while that of N166D opened more but still less than that of the wild type. This open-pore structure could possibly be prevented by unwanted hydrophobic interactions between the three individual mutated residues (*i.e.* Ala or Ile). To explain what caused the wild-type Cry4Ba pore to open, we examined molecules that interact with the three Asn^{166} side-chains on the loops of individual α4-loop-α5 hairpins. It was found that these three side-chains interact with the polar head groups of DMPC lipids as well as water molecules. The partial negative charge (negative dipole) of oxygen atoms (color in red) on Asn^{166} could attract the positively charged choline moiety of DMPC lipids (Fig. 6A, B). Such protein-lipid interactions could thus trigger the opening of the pore.

The number of lipids within 4 Å of the three Asn^{166} residues and their corresponding mutated side-chains were also analyzed (Fig. 6C). It can be seen that both wild-type and N166D pores exhibit an increased

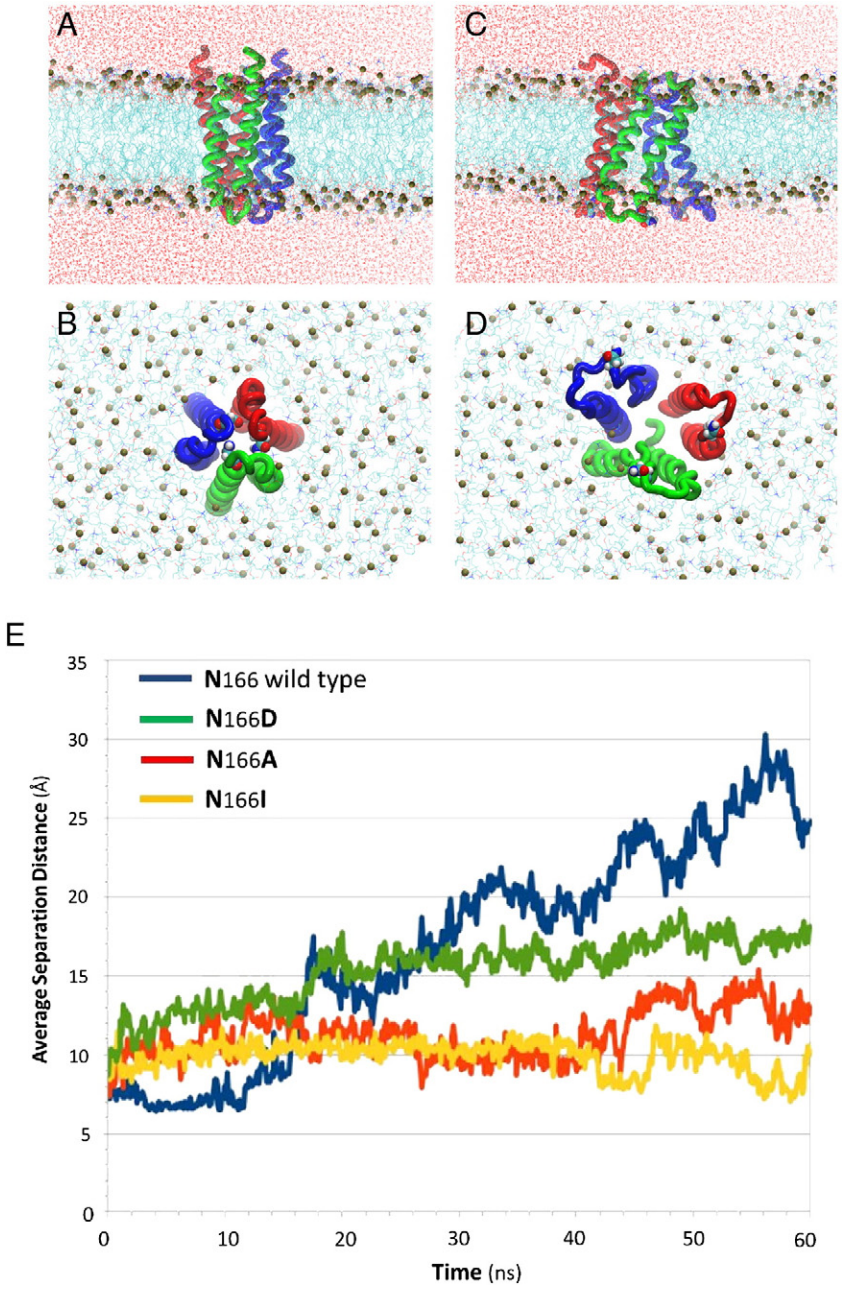

Fig. 5. Opening of the trimeric Cry4Ba pore during 60-ns MD simulations. Snapshots of the MD trajectories (side and bottom views) at time $t = 0$ ns (**A** and **B**) and at time $t = 60$ ns (**C** and **D**). Three α4–α5 hairpins are rendered as tubes. Three Asn^{166} residues and phosphorus atoms of DMPC lipids are drawn as vdW spheres. DMPC lipids (cyan) and water (red) are shown as lines. (**E**) Average separation distance (C_α to C_α) between three Asn^{166} residues on the trimeric Cry4Ba pore and its mutants *versus* time during 60-ns MD simulations.

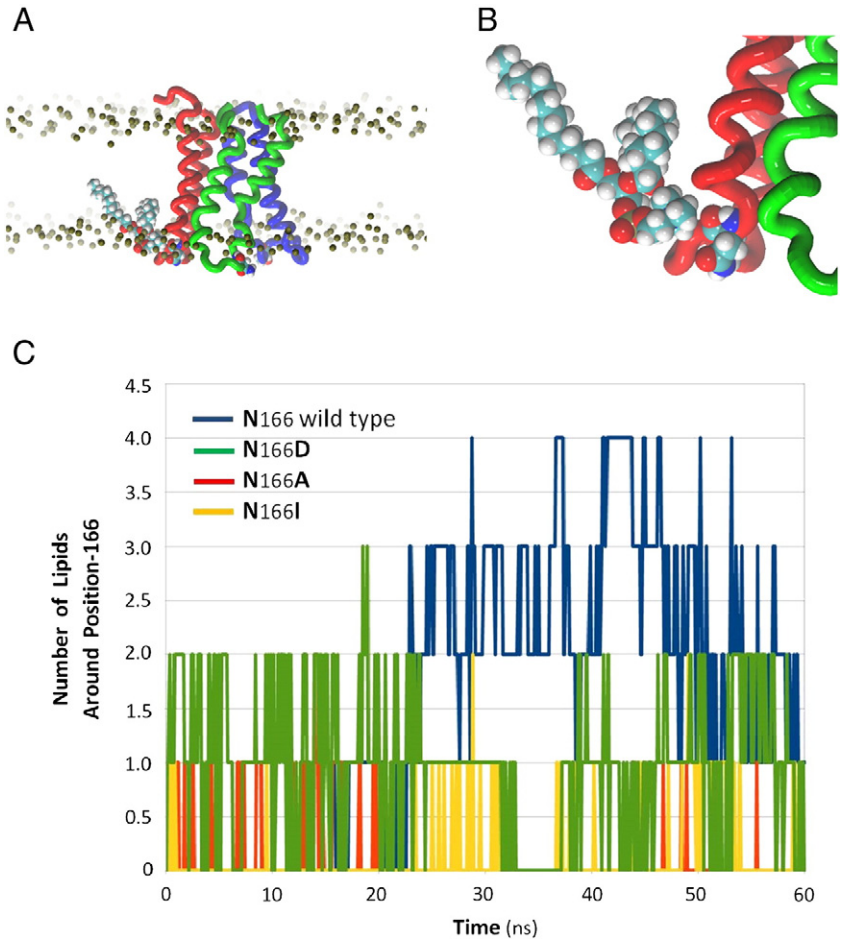

Fig. 6. Interactions between Cry4Ba-166 side chains and DMPC-polar head groups. (A) DMPC lipids within 4 Å of one of Asn^{166} residues on Cry4Ba pore relative to phosphorus layers (gold spheres) of DMPC membrane at time $t = 60$ ns. For clarity, lipids and water are not shown. (**B**) Magnified view of the DMPC lipid interacting with an Asn^{166} residue of the Cry4Ba pore. Both Asn^{166} residues and the DMPC lipid are rendered as vdW spheres and colored by atom names. (**C**) Number of DMPC lipids within 4 Å of three Asn^{166} residues and their mutants on the trimeric Cry4Ba pore *versus* time during 60-ns MD simulations.

number of lipid molecules interacting with them (up to four and two lipids, respectively), while pores containing N166A and N166I have a lower number of lipid molecules around the mutated side-chains (between zero and one). This would indicate that the polarity at the α4–α5 loop position-166 plays an important role in protein–lipid interactions and hence for Cry4Ba-pore opening at the membrane–water interface. As can be also inferred from the Cry4Ba-pore model, Asn^{166} basically faces the pore lumen and the interfacial regions of the membrane. Therefore, substitutions with a non-polar residue could directly affect its interactions with surrounding water and lipids, thus having an adverse effect on conformational changes.

In conclusion, our present results provide more insight into the functional significance of the α4–α5 loop residue—Asn^{166} within the Cry4Ba pore-forming domain. We have demonstrated that the polarity of Cry4Ba-Asn^{166} is essentially involved in ion permeation through the toxin-induced pore and likely promotes the toxin-pore opening. Similarly, the presence of a polar side-chain in the α4–α5 loop might possibly be a general requirement for pore formation of other Cry toxins. For instance, either Glu^{151} or Asn^{152} located in this loop of the Cry1Aa toxin (Fig. 1B) could be a candidate to represent the corresponding polar residue in the Cry4Ba toxin with the conserved function of Asn^{166} (see Supplementary Fig. 1). Nevertheless, this notion still needs to be elucidated. Further studies on toxin-induced pore architecture and mechanism of ion passage through the channel pore would also be of great interest. A detailed understanding of the structural basis for ion permeable-pore formation by this mosquito-active toxin is very imperative since this will bolster the development of engineered biopesticides for the control of human-disease vectors.

Supplementary data to this article can be found online at http://dx.doi.org/10.1016/j.bbamem.2013.10.002.

Acknowledgements

This work was supported in part by the grants from the Thailand Research Fund (TRF). The Royal Golden Jubilee — PhD scholarship from TRF (to T.J.) is gratefully acknowledged. We are also grateful to Witchukorn Phuthong for help with trimeric pore modeling.

References

[1] E. Schnepf, N. Crickmore, J. van Rie, D. Lereclus, J. Baum, J. Feitelson, D.R. Zeigler, D.H. Dean, *Bacillus thuringiensis* and its pesticidal crystal proteins, Microbiol. Mol. Biol. Rev. 62 (1998) 775–806.
[2] B.A. Federici, H.-W. Park, D.K. Bideshi, Overview of the basic biology of *Bacillus thuringiensis* with emphasis on genetic engineering of bacterial larvicides for mosquito control, Open Toxinol. J. 3 (2010) 83–100.
[3] C. Angsuthanasombat, Structural basis of pore formation by mosquito-larvicidal proteins from *Bacillus thuringiensis*, Open Toxinol. J. 3 (2010) 119–125.
[4] L. Regis, M.H. Silva-Filha, C. Nielsen-LeRoux, J.F. Charles, Bacteriological larvicides of dipteran disease vectors, Trends Parasitol. 17 (2001) 377–380.
[5] C.R. Pigott, D.J. Ellar, Role of receptors in *Bacillus thuringiensis* crystal toxin activity, Microbiol. Mol. Biol. Rev. 71 (2007) 255–281.
[6] L. Pardo-López, M. Soberón, A. Bravo, *Bacillus thuringiensis* insecticidal three-domain Cry toxins: mode of action, insect resistance and consequences for crop protection, FEMS Microbiol. Rev. 37 (2013) 3–22.

[7] P. Boonserm, P. Davis, D.J. Ellar, J. Li, Crystal structure of the mosquito-larvicidal toxin Cry4Ba and its biological implications, J. Mol. Biol. 348 (2005) 363–382.
[8] P. Boonserm, M. Mo, C. Angsuthanasombat, J. Lescar, Structure of the functional form of the mosquito larvicidal Cry4Aa toxin from *Bacillus thuringiensis* at a 2.8-Angstrom resolution, J. Bacteriol. 188 (2006) 3391–3401.
[9] J. Li, J. Carroll, D.J. Ellar, Crystal structure of insecticidal delta-endotoxin from *Bacillus thuringiensis* at 2.5 Å resolution, Nature 353 (1991) 815–821.
[10] R.J. Morse, T. Yamamoto, R.M. Stroud, Structure of Cry2Aa suggests an unexpected receptor binding epitope, Structure 9 (2001) 409–417.
[11] P. Grochulski, L. Masson, S. Borisova, M. Pusztai-Carey, J.L. Schwartz, R. Brousseau, M. Cygler, *Bacillus thuringiensis* CryIA (a) insecticidal toxin: crystal structure and channel formation, J. Mol. Biol. 254 (1995) 447–464.
[12] S.L. Slatin, C.K. Abrams, L. English, Delta-endotoxins form cation-selective channels in planar lipid bilayers, Biochem. Biophys. Res. Commun. 169 (1990) 765–772.
[13] O. Peyronnet, V. Vachon, J.L. Schwartz, R. Laprade, Ion channels induced in planar lipid bilayers by the *Bacillus thuringiensis* toxin Cry1Aa in the presence of gypsy moth (*Lymantria dispar*) brush border membrane, J. Membr. Biol. 184 (2001) 45–54.
[14] O. Peyronnet, B. Nieman, F. Généreux, V. Vachon, R. Laprade, J.L. Schwartz, Estimation of the radius of the pores formed by the *Bacillus thuringiensis* Cry1C delta-endotoxin in planar lipid bilayers, Biochim. Biophys. Acta 1567 (2002) 113–122.
[15] B.H. Knowles, Mechanism of action of *Bacillus thuringiensis* insecticidal δ-endotoxins, Adv. Insect Physiol. 24 (1994) 275–308.
[16] E. Gazit, P. La Rocca, M.S. Sansom, Y. Shai, The structure and organization within the membrane of the helices composing the pore-forming domain of *Bacillus thuringiensis* δ-endotoxin are consistent with an "umbrella-like" structure of the pore, Proc. Natl. Acad. Sci. U. S. A. 95 (1998) 12289–12294.
[17] L. Masson, B.E. Tabashnik, Y.B. Liu, R. Brousseau, J.L. Schwartz, Helix 4 of the *Bacillus thuringiensis* Cry1Aa toxin lines the lumen of the ion channel, J. Biol. Chem. 274 (1999) 31996–32000.
[18] I. Sramala, S. Leetachewa, C. Krittanai, G. Katzenmeier, S. Panyim, C. Angsuthanasombat, Charged residues screening in helix 4 of the *Bacillus thuringiensis* Cry4B toxin reveals a critical residue for larvicidal activity, J. Biochem. Mol. Biol. Biophys. 5 (2001) 219–225.
[19] M. Nunez-Valdez, J. Sánchez, L. Lina, L. Güereca, A. Bravo, Structural and functional studies of α-helix 5 region from *Bacillus thuringiensis* Cry1Ab δ-endotoxin, Biochim. Biophys. Acta 1546 (2001) 122–131.
[20] S. Likitvivatanavong, G. Katzenmeier, C. Angsuthanasombat, Asn^{183} in α5 is essential for oligomerisation and toxicity of the *Bacillus thuringiensis* Cry4Ba toxin, Arch. Biochem. Biophys. 445 (2006) 46–55.
[21] S. Leetachewa, G. Katzenmeier, C. Angsuthanasombat, Novel preparation and characterization of the α4-loop-α5 membrane perturbing peptide from the *Bacillus thuringiensis* Cry4Ba toxin, J. Biochem. Mol. Biol. 39 (2006) 270–277.
[22] D. Gerber, Y. Shai, Insertion and organization within membranes of the δ-endotoxin pore-forming domain, helix 4-loop-helix 5, and inhibition of its activity by a mutant helix 4 peptide, J. Biol. Chem. 275 (2000) 23602–23607.
[23] W. Pornwiroon, G. Katzenmeier, S. Panyim, C. Angsuthanasombat, Aromaticity of Tyr-202 in the α4–α5 loop is essential for toxicity of the *Bacillus thuringiensis* Cry4A toxin, J. Biochem. Mol. Biol. 37 (2004) 292–297.
[24] Y. Kanintronkul, I. Sramala, G. Katzenmeier, S. Panyim, C. Angsuthanasombat, Specific mutations within the α4–α5 loop of the *Bacillus thuringiensis* Cry4B toxin reveal a crucial role for Asn-166 and Tyr-170, Mol. Biotechnol. 24 (2003) 11–20.
[25] X.J. Chen, A. Curtiss, E. Alcantara, D.H. Dean, Mutations in domain I of *Bacillus thuringiensis* δ-endotoxin Cry1Ab reduce the irreversible binding of toxin to *Manduca sexta* brush border membrane vesicles, J. Biol. Chem. 270 (1995) 6412–6419.
[26] K. Tiewsiri, C. Angsuthanasombat, Structurally conserved aromaticity of Tyr^{249} and Phe^{264} in helix 7 is important for toxicity of the *Bacillus thuringiensis* Cry4Ba toxin, J. Biochem. Mol. Biol. 40 (2007) 163–171.
[27] K. Tiewsiri, W. Fischer, C. Angsuthanasombat, Lipid-induced conformation of helix 7 from the pore-forming domain of the *Bacillus thuringiensis* Cry4Ba toxin: implications for toxicity mechanism, Arch. Biochem. Biophys. 482 (2009) 17–24.
[28] C. Lailak, T. Khaokhiew, C. Promptmas, B. Promdonkoy, K. Pootanakit, C. Angsuthanasombat, *Bacillus thuringiensis* Cry4Ba toxin employs two receptor-binding loops for synergistic interactions with Cyt2Aa2, Biochem. Biophys. Res. Commun. 435 (2013) 216–221.
[29] T. Glover, K. Mitchell, Testing the difference between two means of independent samples, international ed, in: T. Glover, K. Mitchell (Eds.), An Introduction to Biostatistics, 2nd ed., Waveland Pr. Inc., 2008.
[30] R.J. Mrsny, J.J. Volwerk, O.H. Griffith, A simplified procedure for lipid phosphorus analysis shows that digestion rates vary with phospholipid structure, Chem. Phys. Lipids 39 (1986) 185–191.
[31] T. Puntheeranurak, P. Uawithya, L. Potvin, C. Angsuthanasombat, J.L. Schwartz, Ion channels formed in planar lipid bilayers by the diptheran-specific Cry4Ba *Bacillus thuringiensis* and its α1–α5 fragment, Mol. Membr. Biol. 21 (2004) 67–74.
[32] D.W. Ritchie, D. Kozakov, S. Vajda, Accelerating and focusing protein–protein docking correlations using multi-dimensional rotational FFT generating functions, Bioinformatics 24 (2008) 1865–1873.
[33] S. Jo, J.B. Lim, J.B. Klauda, W. Im, CHARMM-GUI membrane builder for mixed bilayers and its application to yeast membranes, Biophys. J. 97 (2009) 50–58.
[34] W. Humphrey, A. Dalke, K. Schulten, VMD: visual molecular dynamics, J. Mol. Graph. 14 (1996) 27–28.
[35] J.C. Phillips, R. Braun, W. Wang, J. Gumbart, E. Tajkhorshid, E. Villa, C. Chipot, R.D. Skeel, L. Kalé, K. Schulten, Scalable molecular dynamics with NAMD, J. Comput. Chem. 26 (2005) 1781–1802.
[36] K. Marheineke, S. Grunewald, W. Christie, H. Reilander, Lipid composition of *Spodoptera frugiperda* (*Sf*9) and *Trichoplusia ni* (*Tn*) insect cells used for baculovirus infection, FEBS Lett. 441 (1998) 49–52.
[37] P. Ounjai, V.M. Unger, F.J. Sigworth, C. Angsuthanasombat, Two conformational states of the membrane-associated *Bacillus thuringiensis* Cry4Ba delta-endotoxin complex revealed by electron crystallography: implications for toxin-pore formation, Biochem. Biophys. Res. Commun. 361 (2007) 890–895.
[38] C.-Y. Kao, F.C.O. Los, D.L. Huffman, S. Wachi, N. Kloft, M. Husmann, V. Karabrahimi, J.L. Schwartz, A. Bellier, C. Ha, Y. Sagong, H. Fan, P. Ghosh, M. Hsieh, C.-S. Hsu, L. Chen, R.V. Aroian, Global functional analyses of cellular responses to pore-forming toxins, PLoS Pathog. 7 (2011) e1001314.
[39] M. Bali, M.H. Akabas, Gating-induced conformational rearrangement of the γ aminobutyric acid type A receptor β-α subunit interface in the membrane-spanning domain, J. Biol. Chem. 287 (2012) 27762–27770.
[40] D. Colquhoun, R. Lape, Conformational coupling in ion channels: allosteric coupling in ligand-gated ion channels, J. Gen. Physiol. 140 (2012) 599–612.
[41] M. Marchioretto, M. Podobnik, M.D. Serra, G. Anderluh, What planar lipid membranes tell us about the pore-forming activity of cholesterol-dependent cytolysins, Biophys. Chem. (2013), http://dx.doi.org/10.1016/j.bpc.2013.06.015.
[42] C. Muñóz-Garay, L. Portugal, L. Pardo-López, N. Jiménez-Juárez, I. Arenas, I. Gómez, R. Sánchez-López, R. Arroyo, A. Holzenburg, C.G. Savva, M. Soberón, A. Bravo, Characterization of the mechanism of action of the genetically modified Cry1AbMod toxin that is active against Cry1Ab-resistant insects, Biochim. Biophys. Acta 1788 (2009) 2229–2237.
[43] T. Puntheeranurak, C. Stroh, R. Zhu, C. Angsuthanasombat, P. Hinterdorfer, Structure and distribution of the *Bacillus thuringiensis* Cry4Ba toxin in lipid membranes, Ultramicroscopy 105 (2005) 115–124.
[44] N. Groulex, H. McGuire, R. Laprade, J.L. Scheartz, R. Blunck, Single molecule fluorescence study of the *Bacillus thuringiensis* toxin Cry1Aa reveals tetramerization, J. Biol. Chem. 286 (2011) 42274–42282.
[45] D.V. McAllister, P.M. Wang, S.P. Davis, J.-H. Park, P.J. Canatella, M.G. Allen, M.R. Prausnitz, Microfabricated needles for transdermal delivery of macromolecules and nanoparticles: fabrication methods and transport studies, Proc. Natl. Acad. Sci. U. S. A. 100 (2003) 13755–13760.